Electron. Mater. Lett., Vol. 12, No. 1 (2016), pp. 178-185
DOI: 10.1007/s13391-015-5095-9

Influence of Phosphorous Content on Microstructure Development at the Ni-P Plating/SAC Interface

Zbigniew Huber,[1] Joanna Wojewoda-Budka,[2,*] Anna Wierzbicka-Miernik,[2] Anna Sypien,[2] Maciej Szczerba,[2] and Pawel Zieba[2]

[1]Fideltronik Poland Ltd., Beniowskiego 1, 34-200 Sucha Beskidzka, Poland
[2]Institute of Metallurgy and Materials Science, Polish Academy of Sciences, 25 Reymonta St., 30-059 Cracow, Poland

(received date: 3 March 2015 / accepted date: 5 October 2015 / published date: 10 January 2016)

Studies of the commonly used Ni-P surface finish of 4.3 and 11.6 wt. % of P content electroless plated on nickel substrates followed by their reaction with SAC305 solder were performed. It was demonstrated that the Ni-4.3P plating was crystalline, while the Ni-11.6P was mostly amorphous. The transformation of the Ni-P into Ni_3P phase took place at 672 K and 605 K for low and high P amount, respectively. The activation energy (E_a) of the crystallization processes in the Ni-P plating was lower for the Ni-11.6P plating. Interaction of SAC305 solder with both types of the inspected plating showed the creation of $(Cu,Ni)_6Sn_5$ phase in the form of thin layer and large scallops, while for Ni-11.6P/SAC305 interface also $(Ni,Cu)_3Sn_4$ phase. The thickness of these phases was larger in the case of low phosphorous containing plating. The Ni-11.6P plating after the reaction with SAC305 totally transformed into $Ni_{12}P_5$, while the enrichment in P up to 10.5 wt. % occurred in the Ni-4.3P which did not lead to the appearance of any Ni_xP_y type phases. After the reaction of plating with solder the Ni_2SnP phase was not identified. This was related to the absence of spalling phenomenon of the intermetallics into solder.

Keywords: Ni-P electroless plating, intermetallic phases, lead-free soldering, SAC solder

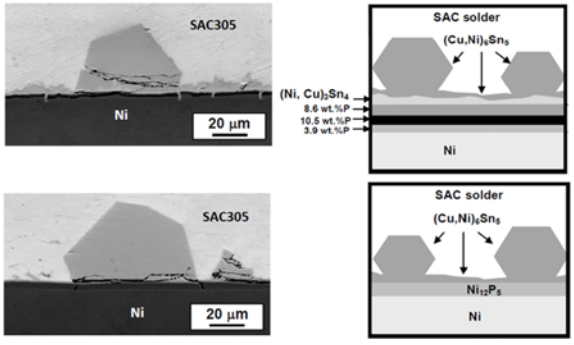

1. INTRODUCTION

The progress in electronics and continuous component miniaturisation requires solder interconnections and solder land size reduction on the printed circuit board (PCB). In order to provide a coplanar and solderable land surface, various finishes are used; for high density designs, one of the most common is Electroless Nickel Immersion Gold (ENIG). The finish is compatible with the eutectic lead-based and lead-free solder alloys.

The ENIG finish contains a nickel layer deposited directly onto a copper solder land via electroless process and a thin gold layer protecting the nickel surface against oxidation. According to electronics industry standard IPC-4552 the nickel layer thickness is specified between 3 - 6 μm and the gold layer should be 0.05 μm minimum. The deposition of gold exceeding 0.125 μm could result in nickel corrosion often referred to as galvanic hyper-corrosion of the electroless plated nickel by the gold plating bath.[1]

Subsequent soldering processes dissolve gold in the solder alloy and the corroded nickel is exposed. The effect is known as a black pad. Apart from the galvanic hyper-corrosion of the nickel layer, there are other factors that may

*Corresponding author: j.wojewoda@imim.pl

cause the nickel surface degradation or corrosion like incomplete solder mask curing prior to ENIG, the influence of solder land pattern designs or variation of phosphorus in the nickel layer. The latter one was to some extent considered in the literature,[2-10] however, there is still lack of systematic studies of the influence of phosphorous content on microstructure changes (e.g. phase transformations) occurring in the near-interface region.

The goal of the present study was to provide more details about the correlation between the phosphorus content in the Ni-P plating layer and its behaviour after reaction with SnAgCu lead-free solder.

2. EXPERIMENTAL PROCEDURE

Nickel substrates were electroless covered with about 5 μm thick Ni-P layers consisting of 4.3 (Ni-4.3P) and 11.6 (Ni-11.6P) wt. % of phosphorous. The microstructure of Ni-P layers was examined using scanning electron microscopes (SEM) FEI E-SEM XL30 and Quanta 3D equipped with an energy dispersive x-ray spectrometer (EDS) EDAX Gemini for microchemical analysis. Differential scanning calorimeter (DSC) 404 F1 Pegasus (Netzsch company) was applied to determine the temperature of phase transformations within the Ni-P plating. The measurements were performed with the continuous heating process at different constant rates of 2, 5, 10 and 20 K/min in a pure argon protective atmosphere. The analysis of the thermal peaks was performed with the Netzsch integrated software Proteus 6.0. X-ray diffraction (XRD) measurements were carried out with Bruker D-8 Discover diffractometer using filtered Co K_α radiation in order to compare the crystalline structure of all samples.

The reaction between Ni-P plating and SAC305 solder paste (Alpha Metals 96.5Sn3.0Ag0.5Cu wt. %) took place in the sessile drop test at 508 K for 5 minutes. After that, the microstructure (plane view and cross-section) were investigated using SEM/EDS in order to check both the changes within the Ni-P plating and the phase composition of the Ni-P/SAC305 interface.

3. RESULTS

3.1 Ni-P plating

The starting point of the examination was to get comprehensive information about the Ni-P plating, which could clearly demonstrate the differences between the two applied phosphorous contents: 4.3 wt. % and 11.6 wt. %. The SEM observations (Fig. 1a,b) showed mud type of surface morphology of both types of plating. For the higher phosphorous content the bubbles were equally distributed, while the Ni-4.3P sample presented a more smooth surface with groups of bubbles only.

The x-ray diffraction patterns taken for the both types of Ni-P plating are presented in Fig. 1c. The Ni-P plating within the Ni/Ni-4.3%P sample (i.e. smaller P content) can be characterized as partly crystalline with the grain size measured from the width of main {111} reflection to be about 16 nm. On the other hand, the Ni-P plating of the higher nominal P content sample is amorphous. In this case, the contribution of the Ni-P layer in the XRD pattern manifests itself as the broad background, typical for amorphous materials which is observed in the vicinity of the sharp {111} peak. As the x-rays can easily penetrate the thin Ni-P layer, thus, the sharp {111} peak and others observed at higher 2theta values come from the bulk coarse grained Ni sample being below the Ni-P layer.

As a next step, the DSC technique was applied to detect the changes, which appeared within the plating during the experiment. Figure 2 represents the DSC curves of Ni-4.3P and Ni-11.6P Ni-P plating on nickel substrate. Both curves

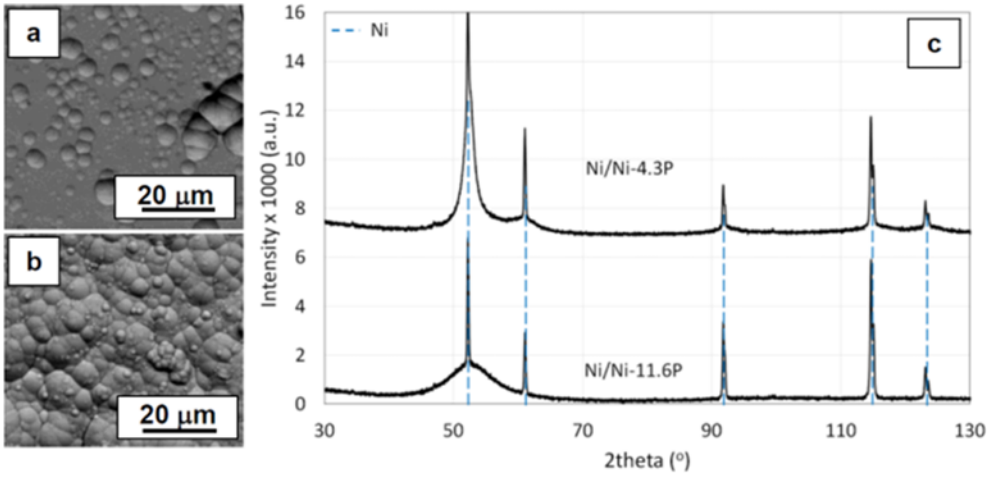

Fig. 1. The SEM (BSE) images of the Ni-P plating surfaces obtained for: Ni-4.3P (a) and Ni-11.6P plating (b) together with the XRD patterns for Ni-P plating covering Ni substrate of both phosphorous content (4.3 and 11.6 wt. %) (c).

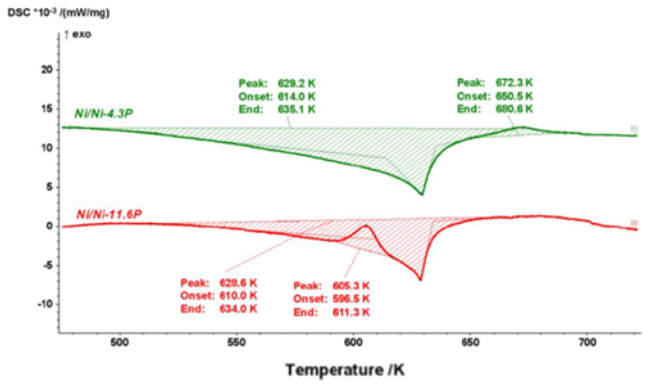

Fig. 2. The DSC curves obtained for Ni-4.3P and Ni-11.6P plating.

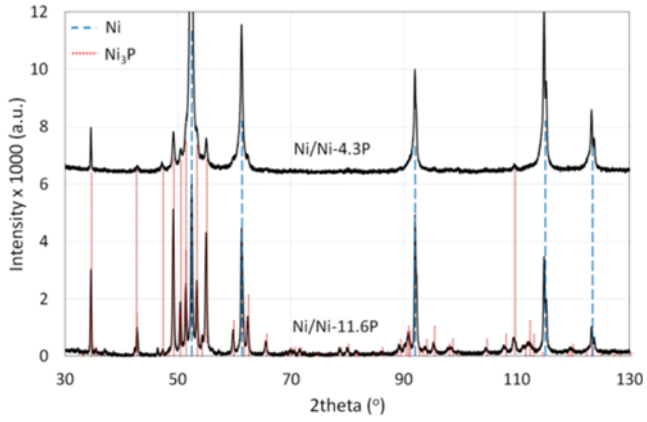

Fig. 3. The XRD patterns obtained for Ni-P plating on Ni substrate of both phosphorous contents (4.3 and 11.6 wt. %) after DSC experiment.

show the endothermic peak at about 629 K related to the magnetic transition of the Ni base material. However, the presence of the exothermic peak appearing at various temperatures could also be noticed. For the Ni-4.3P plating, it was detected at 672 K, while for the Ni-11.6P it was localized at much lower temperature of 605 K. This peak (also called as crystallization peak) is related to the phase transformation of Ni-P plating into stable Ni and Ni_3P.

The samples of both types of plating after the DSC experiments were again examined using XRD technique in order to confirm the presence of Ni_3P phase, which crystallized during the heating process (Fig. 3). The presence of Ni_3P phase can be clearly observed in both types of samples.

3.2 Ni-P/SAC interaction

The SEM analysis after the reaction of Ni-P plating with SAC305 solder clearly showed large amount of cracks within the Ni-4.3P plating (Fig. 4a). After the interaction of SAC305 solder with Ni-P plating of higher phosphorous content, the plating surface was free from cracks while the bubbles could be more easily distinguished in comparison with the Ni-4.3P plating (Fig. 4b).

The interface between SAC305 and Ni-P plating of both phosphorous contents is showed in Fig. 5, where the presence of the intermetallic phases can be observed in the shape of continuous layers or big faceted scallops. It is worth mentioning that the spalling phenomenon of the intermetallic phases was not observed at all, however within the scallops the cracks were distinguished. Monitoring of the chemical composition changes in different microstructure areas was performed and the results are collected in Table 1. The intermetallic layer of bright grey colour (denoted further in the text as IMC1) is present in the form of either the scallops (point 1 in Fig. 5c and Table 1) or the layer (point 2 in Fig. 5c and Table 1). Below the IMC1 the second intermetallic phase, denoted as IMC2, could be distinguished in the case of Ni-4.3P plating (point 3 in Fig. 5c and Table 1).

Significant differences were observed for both types of samples, since the presence of the cracks within the Ni-P plating was more evident in the case of lower phosphorus

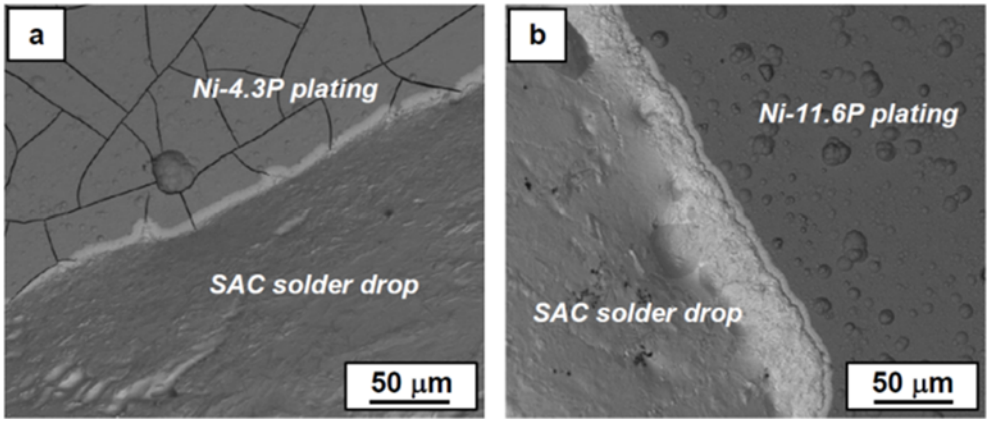

Fig. 4. The SEM (BSE) images of the Ni-P plating surfaces after interaction with the SAC305 solder obtained for: Ni-4.3P (a) and Ni-11.6P (b).

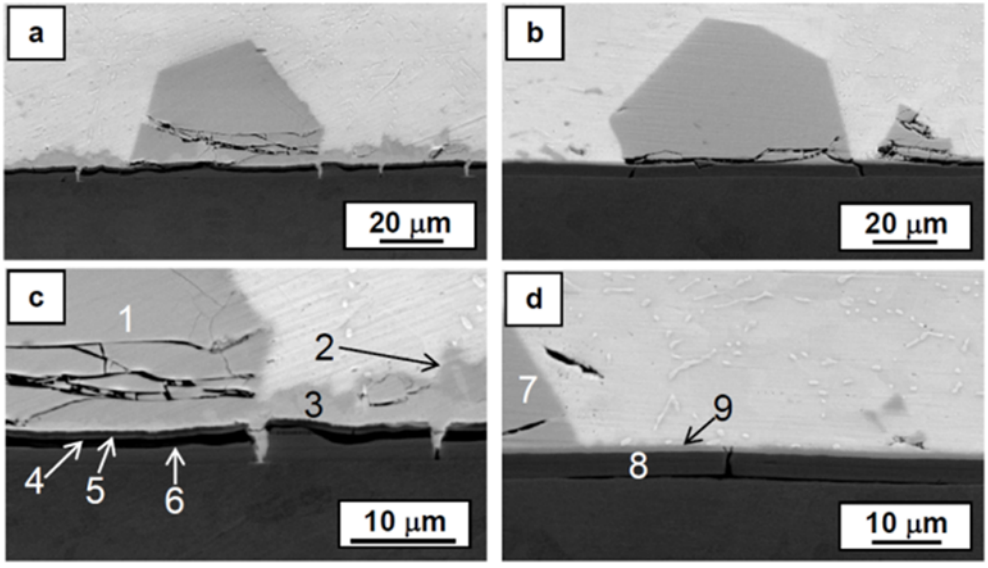

Fig. 5. The SEM (BSE) images of the Ni/Ni-P/SAC305 cross sections obtained for: Ni-4.3P (a,c) and Ni-11.6P (b,d). Numbers denote the characteristic places of chemical composition analyses (see Table 1).

Table 1. Results of the chemical analysis measured with EDS at the places marked with numbers in Figures 5c (Ni/Ni-4.3P/SAC305) and 5d (Ni/Ni-11.6P/SAC305).

Fig. 5c	Weight %	Atomic %	Phase
1	62.6Sn + 16.6Ni + 28.8Cu	46.4Sn + 24.9Ni + 28.7Cu	$(Cu,Ni)_6Sn_5$
2	59.5Sn + 15.5Ni + 25Cu	43.3Sn + 22.7Ni + 34Cu	$(Cu,Ni)_6Sn_5$
3	70Sn + 23Ni + 7Cu	54.1Sn + 35.9Ni + 10Cu	$(Ni,Cu)_3Sn_4$
4	10.5P + 2.8Sn + 86.7Ni	18.5P + 1.3Sn + 80.2Ni	Ni-P plating
5	8.6P + 1.8Sn + 89.6Ni	15.3P + 0.8Sn + 83.9Ni	Ni-P plating
6	3.9P + 96.1Ni	7.1P + 92.9Ni	Ni-P plating
Fig. 5d	Weight %	Atomic %	Phase
7	59.7Sn + 15.6Ni + 24.7Cu	43.5Sn + 23Ni + 33.6Cu	$(Cu,Ni)_6Sn_5$
8	17.6P + 82.4Ni	28.8P + 71.2Ni	$Ni_{12}P_5$
9	17.9P + 4.8Sn + 77.3Ni	29.9P + 2.1Sn + 68Ni	$Ni_{12}P_5$

electroless plating.

The variations of contrast observed using backscattered electrons mode in SEM within the Ni-P plating layer after the reaction with SAC305 solder were noticed for plating with lower phosphorous content, where at least three sublayers existed (Fig. 5c and Table 1-points 4, 5 and 6). On the other hand, the changes in the plating layer in the Ni-11.6P/SAC305 sample came down to the formation of a single $Ni_{12}P_5$ phase consisting of 17.2 ÷ 17.9 wt. % P (Fig. 5d and Table 1-point 8). The sample with lower phosphorous content exhibited phosphorous composition changes within the Ni-P plating from 3.9 ÷ 10.5 wt. %, which most probably could lead to the formation of one of the Ni-P phases due to the subsequent heating process.

4. DISCUSSION

4.1 Ni-P plating

The comprehensive information was gathered concerning the Ni-P plating of two phosphorous contents: 4.3 wt. % and 11.6 wt. % using various techniques such as scanning electron microscopy, x-ray diffraction technique and differential scanning calorimetry, in order to find the differences between the electroless finish before the reaction with SAC305 solder. The microstructures of the plating surfaces revealed typical mud-type morphology. Moreover, analysing the XRD spectra, it can be deduced from the shape of the first peak occurring in the diffractogram that in the case of Ni-11.6P plating is mostly amorphous. On the other

hand, the low phosphorous plating can be described as crystalline with a mean grain size of 16 nm. The XRD results are in agreement with the data of Park *et al*.,[4] who examined the Ni-P consisting of 10.1 wt. % P and described such plating to have grains of 4 - 5 nm, while its electron diffraction pattern had amorphous characteristics.

The crystallization temperature of Ni-P plating previously reported in the literature varied widely from 573 to 723 K depending on the phosphorous content (1.9 - 13.6 wt. %).[2-6] Hur *et al*.[5] reported the presence of the peak correlated with the crystallization of the Ni_3P phase at 673 K for 6.3 wt. % P in Ni-P plating while for 11.5 wt. % P two peaks corresponded to the formation of Ni and Ni_3P crystallites. Our results differ from those obtained by Hur *et al*.[5] – the temperatures of crystallization peak are significantly higher (peak at ~673 K for 4.3 wt. % P (our) contrary to 6.3 wt. % P (Hur *et al*.) and peak at either 605 (our) or 623 K (Hur *et al*.) for almost the same composition ~11.5 wt. % P). Such discrepancies arose from various heating rates, which could significantly influence the crystalline transition temperature.[11] However, the crystallization temperature of the Ni-4.6P film measured by

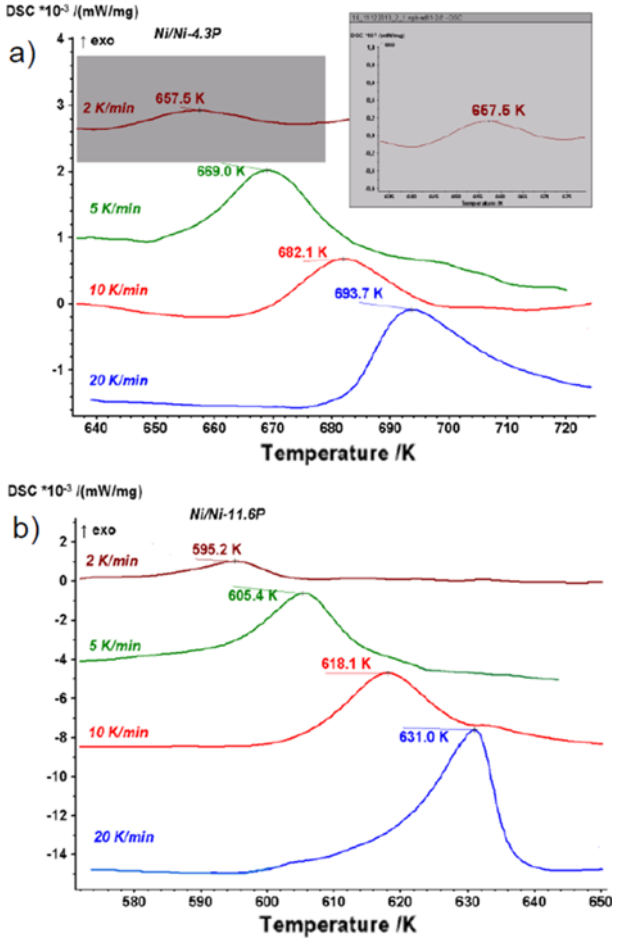

Fig. 6. The DSC curves for Ni-4.3P (a) and Ni-11.6P (b) plating obtained using 2, 5, 10 and 20 K/min heating rates.

Sohn *et al*.[3] at the same heating rate was 654.3 K, which shows how much the Ni-P plating depended on the phosphorous content, especially when the P amount was low. The comparison of our results and Sohn's *et al*.[3] together with the results obtained by Hur *et al*.[5] suggests that the crystallization temperature measured for lower phosphorous content plating is much more sensitive to the chemical composition variation than in the case of high amounts of P in Ni-P plating, because of different crystallization mechanisms.

The correlation between the phosphorous content and the temperature of the crystallization of the Ni-P plating is especially important when choosing the soldering method. Rising the phosphorous content in the plating, causes lowering the temperature at which the crystalline phase will occur. This is particularly important during the manual soldering, when the alloy temperature may exceed 573 K, because of the fact that the solder iron tip temperature is usually set up to 623 - 673 K, depending on solder alloy type, soldering iron power and its ability to transfer the heat from the solder tip onto solder land and component connection surfaces.

Furthermore, the application of various heating rates in DSC experiment for both types of electroless plated Ni-P allowed the determination of the activation energy of crystallization (E_a). Figure 6 presents the DSC curves obtained at heating rates of 2, 5, 10 and 20 K/min for both types of plating without the magnetic transition being automatically subtracted using the analytical software.

Increasing heating rates causes the shift of the temperature of the crystallization (T_p) towards higher temperatures. The values of the crystallization activation energy (E_a) were calculated based on the Duswalt model[12] (Eq. (1)):

$$E_a \approx -R \cdot (d(\ln\beta)/d(1/T_p)) \quad (1)$$

as well as Kissinger's model[13] (Eq. (2))

$$\ln(\beta/T_p^2) = -E_a/RT_p + \ln(K_o E_a/R) \quad (2)$$

where R – gas constant (8.314 J/Kmol), β – heating rate (K/min), T_p – peak temperature (K), the $\ln(K_o E_a/R)$ in Eq. (2) is constant.

From the slope of the straight lines (Eqs. (1) and (2)) presented in Fig. 7 it is possible to derive the values of the activation energy, E_a.

Figures 7a and 7b show the relationship between the heating rate and temperature of crystallization derived from Eq. (1) and Eq. (2), respectively.

The activation energy values are collected in Table 2.

The activation energy of Ni-4.3P plating, calculated by both Duswalt and Kissinger models, was higher than that for the high phosphorus one. These results are in agreement

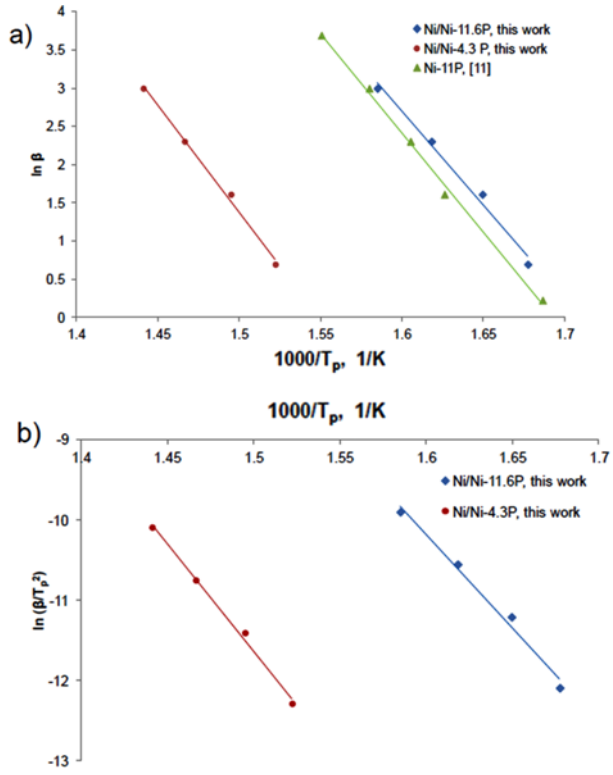

Fig. 7. Relationship between the heating rates (β) and temperature of crystallization (T_p) for the determination of activation energy of crystallization (E_a) for both types of plating based on Duswalt model compared with literature data [11] (a) and Kissinger model (b).

Table 2. Activation energy values obtained for both type of plating compared to the literature data.[11,14]

P [wt. %]	E_a [kJ/mol]		Ref.
	Duswalt model (Eq. (1))	Kissinger model (Eq. (2))	
4.3	232.4 ± 10.8	221.2 ± 10.8	This work
11.6	203.8 ± 15.8	193.6 ± 15.8	This work
11	227.6	-	[11]
10-14	-	225 ± 20	[14]
0	289 (E_a of self-diffusion in pure Ni)		[14]

within the error limits with the values reported by Mahoney[11] as well as Keong.[14] In addition, comparing the results with the activation energy for self-diffusion for pure Ni, the strong dependence between the phosphorous content and the crystallization activation energy is indicated - lower P content plating has higher E_a. This correlation should be taken into account during the soldering process because due to the lower activation energy the crystallization process will occur more easily.

The XRD spectra of both types of plating after the DSC experiment confirmed the presence of Ni_3P phase, which crystallized during the heating process. The experiment concerning the Ni-P plating after DSC was also reported by Keong *et al.*[14] They found the presence of amorphous phase, nickel and Ni_3P phase after heating up to 773 K on the plating containing 10 ÷ 14 wt. % P. On the other hand, heating up to 673 K resulted in the additional formation of Ni_2P and $Ni_{12}P_5$ metastable phases. Also Hur *et al.*[5] observed Ni_3P crystalline peaks of the Ni-P deposit after annealing at 723 K as being the only phase present in the plating. It was evidenced that despite the composition of the Ni-P plating the final products were Ni_3P and Ni crystallites, however, the phase transformation path can go through the Ni_xP_y metastable phases formation. Hur *et al.*[5] concluded that the Ni-11.5P plating was the most stable amorphous phase resistant to the changes in the structure, where the formation of only Ni_3P and Ni crystallites was observed.

4.2 Ni-P/SAC interaction

Scanning electron microscopy observation combined with chemical composition analysis allowed drawing a schematic model of the interface changes occurring due to the interaction of Ni-P plating with SAC305 solder (see Fig. 8).

The cracks observed for low P content plating after reaction with SAC305 probably aroused due to the stresses present within the electroless cover, especially if the structure of such plating was of nanocrystalline type. In the case of higher phosphorous content the amorphous structure enables the relaxations of the stresses occurring during the plating process, therefore no cracks were observed in the case of Ni-11.6P plating. It is also worth to mention that these cracks (Figs. 4a, 5a, 5c) do not play an important role in the diffusion processes, because if so the morphology around these cracks should resemble the scallop morphology, which is not the case. Moreover, the studies performed by Yoon *et al.*,[15] although for Sn-3.5Ag solder and Ni-P electroless substrate, showed that the growth of Ni_3Sn_4 as well as Ni_3P had power-law relationship indicating that the growth of both these phases is governed by volume diffusion. Therefore, we may suspect that the nickel diffusion in our case goes in the same way, and this is why the cracks do not play an important role.

The microchemical analysis gathered in Table 1 show that the IMC1 could be described as both $(Cu,Ni)_6Sn_5$ and $(Ni,Cu)_3Sn_4$, however, the presented composition falls into $(Cu,Ni)_6Sn_5$ phase field in the 493 K isothermal cross section of Ni-Cu-Sn equilibrium phase diagram presented in [16]. The second intermetallic phase, possible to detect only in Ni-4.3P samples after reaction with solder, was described as $(Ni,Cu)_3Sn_4$. These results are in agreement with the examination of Yoon *et al.*,[17] who identified the same intermetallics at the Sn-0.4Cu/ENIG interface and also observed similar morphology of large and faced scallops, but after 60 minutes of reaction time at 528 K. On the other

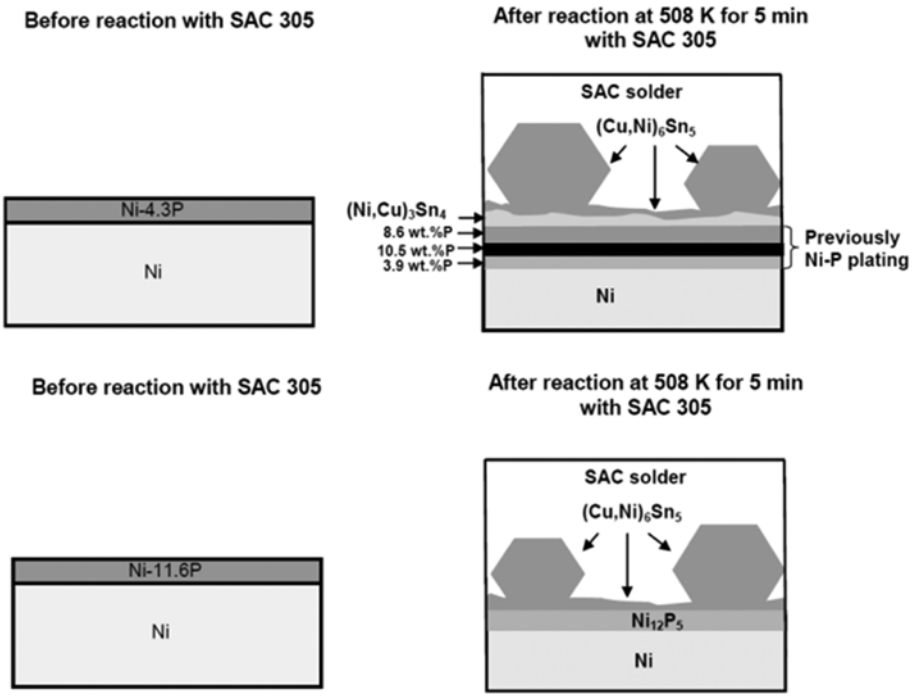

Fig. 8. Schemes of the Ni/Ni-P/SAC305 interface transformation for two variants of phosphorous contents: Ni-4.3 wt. % and Ni-11.6 wt. %.

hand, the second intermetallic phase $(Ni,Cu)_3Sn_4$ formation was reported[2,18] during solid state reaction of plating and pure Sn solder. The presented here experimental results allow the conclusion that larger amount of phosphorous within the applied plating retarded the growth of $(Cu,Ni)_6Sn_5$ and also the formation of Ni_3Sn_4 intermetallic phases.

The plane view microstructures observed for both types of plating differed especially due to the presence or lack of cracks, which were evidenced in the case of lower phosphorus electroless plating. Defects such as voids were observed in [9] within the Ni-7P plating after reaction with SAC and only for this composition among other (10 and 13 wt. % of P) examined samples. Therefore, it seems that with decreasing phosphorous content continuity of the plating could suffer more due to the reaction with solder.

Chemical composition changes within the Ni-P plating after the reaction with SAC305 are in agreement with our previous results concerning ENIG (the commercially used Ni-P plating with thin gold layer on top) and SAC305 interaction at 503 K studied with the aim of transmission electron microscopy.[19]

Wojewoda-Budka *et al*.[19] showed for the experiment with plating containing 6 ÷ 9 wt. % P that several layers existed after reaction with SAC: NiP-amorphous layer corresponding to Ni-P coating, $Ni_{12}P_5$, Ni_2SnP and the intermetallic phases mainly $(Ni,Cu)_3Sn_4$ with some amount of $(Cu,Ni)_6Sn_5$ and Ag_4Sn phases. Presented here results concerning lower (Ni-4.3P) and higher (Ni-11.6P) phosphorous containing plating are in accordance with the one described in [19] experiment. In the case of SAC305/Ni-4.3P, the Ni-P plating was still present, however, the amount of phosphorous increased up to 10.5 wt. % due to the nickel diffusion into the solder followed by the reaction with SAC305 and formation of the intermetallics such as $(Cu,Ni)_6Sn_5$ or/and $(Ni,Cu)_3Sn_4$ phases. In the second type of electroless plating (Ni-11.6P) the reaction with SAC solder resulted in the total transformation of the Ni-P into $Ni_{12}P_5$ phase. Plating, in which the amount of P content was 6 ÷ 9 wt. %[19] could be described as the state in between these two: next to the $Ni_{12}P_5$ layer, the layer rich in phosphorous content is still present. The results of this work show that although the tin content was also detected within the Ni-P layer its amount (less than 2.1 wt. % of Sn) was not sufficient to indicate it as Ni_2SnP phase by means of SEM/EDS. It was previously reported[8] that the formation of the Ni_2SnP phase could be responsible for the spalling of the $(Cu,Ni)_6Sn_5$ intermetallic phases. The studies of Lin *et al*.[7-9] on the phase evolution at the interface between SAC and Ni-P of 7 or 13 wt. % P plating (reflow temperature peak at 513 K) showed the formation of Ni_3P layer between the solder and the Ni–7P UBM. For the Ni-13P the first phase, which occurred was $Ni_{12}P_5$ and only due to further Ni diffusion into $Ni_{12}P_5$ the formation of stable Ni_3P took place. In their studies also a continuous Ni_2SnP layer formed at the interface of the SAC/Ni-13 wt. % P joint, while in the case of SAC/Ni-7 wt. % P joint, only a little amount of Ni_2SnP phase was detected. In the light of the study of Lin *et al*.[7-9] our results extend the existing knowledge and reduce the window of formation of

the $Ni_{12}P_5$ phase from 13 wt. % of P to 11.6 wt. %, where the Ni_2SnP phase is not present in the *micro* scale. On the other hand, for the low phosphorous content plating (4.3 wt. %), the Ni_xP_y phases were not identified, while according to literature the enrichment in P within the Ni-P up to 6 ÷ 8 wt. % caused the formation of either Ni_3P[7-9] or $Ni_{12}P_5$.[19]

Finally, the important remark should be given to the faster growth of IMC as a result of Ni-4.3P and SAC reaction in comparison with the Ni-11.6P/SAC one. It is probably caused by the higher amount of nickel within the plating. Previous studies[20,21] unambiguously demonstrated the strong influence of Ni concentration on the kinetics of the intermetallic phase growth. Even small additives such as 1 - 5 at. % of Ni significantly accelerated the IMC's growth.

5. CONCLUSIONS

The comprehensive studies of the commonly used Ni-P surface finish of two variants of low (4.3 wt. % of P) and high (11.6 wt. % of P) phosphorous content electroless plated revealed the crystalline character of the Ni-4.3P plating, which substantially differed from the Ni-11.6P plating composed of Ni nanocrystallites in the amorphous matrix. The temperature of the Ni-P into Ni_3P phase transformation increased with the decrease in P content and activation energy of the crystallization process was higher for Ni-4.3P plating, which has significant meaning in the sense of thermal cycling working conditions. The presented studies on the early stage of reaction between the Ni-P plating of two compositions and SAC solder falls into widely discussed ENIG/SAC interaction in the literature. First of all, application of nickel substrate covered by Ni-P plating reacting with SAC305 solder resulted in the formation of the intermetallic phases at the interface, although the spalling phenomenon did not take place. It was found that for the low phosphorous containing plating (4.3 wt. % of P) the thicker layer of the intermetallic phases compared with the Ni-11.6P plating was created at the plating/solder interface, which was attributed to the acceleration of the IMC's growth in the case of higher Ni amounts in Ni-4.3P plating. Also, for this type of cover (Ni-4.3P), the occurrence of discontinuities in the Ni-P was observed. The formation of $(Cu,Ni)_6Sn_5$ phase in the form of thin layer and large scallops were detected in the both types of plating, while for Ni-11.6P/SAC interface $(Ni,Cu)_3Sn_4$ phase additionally grew between the plating and $(Cu,Ni)_6Sn_5$ phase. The thickness of these phases was larger in the case of low phosphorous containing plating. It was found that the plating containing 11.6 wt. % of P after the reaction with SAC transformed into solely $Ni_{12}P_5$ phase. Although the tin was detected in small amounts in both types of samples the Ni_2SnP phase was not identified. This could also prove however not explicitly that the presence of Ni_2SnP caused the spalling phenomenon.

ACKNOWLEDGEMENTS

This work has been supported by the Polish Governmental funds and structural funds of EC under Project No UDA-POIG.01.03.01-00-103/09-00 "The improvement of reliability of lead-free solder joints in electronic devices". The experimental studies (SEM, XRD, DSC) were performed in the Accredited Testing Laboratories at the Institute of Metallurgy and Materials Science of the Polish Academy of Sciences.

REFERENCES

1. D. J. Lee and H. S. Lee, *Microelectron. Reliab.* **46**, 1119 (2006).
2. Y. C. Sohn, J. Yu, S. K. Kang, W. K. Choi, and D. Y. Shih, *J. Mater. Res.* **18**, 4 (2003).
3. Y. C. Sohn, J. Yu, S. K. Kang, D. Y. Shih, and W. K. Choi, *J. Electron. Mater.* **33**, 790 (2004).
4. S. H. Park and D. N. Lee, *J. Mater. Sci.* **23**, 1643 (1988).
5. K. H. Hur, J. H. Jeong, and D. N. Lee, *J. Mater. Sci.* **25**, 2573 (1990).
6. T. Hentschel, D. Isheim, R. Kirchheim, F. Muller, and H. Kreye, *Acta Mater.* **48**, 933 (2000).
7. Y. C. Lin, T. Y. Shih, S. K. Tien, and J. G. Duh, *J. Electron. Mater.* **36**, 1469 (2007).
8. Y. C. Lin and J. G. Duh, *Scripta Mater.* **54**, 1661 (2006).
9. Y. C. Lin, *J. Electron. Mater.* **35**, 1665 (2006).
10. Y. C. Lin, K. J. Wang, and J. G. Duh, *J. Electron. Mater.* **39**, 283 (2010).
11. M. W. Mahoney and P. J. Dynes, *Scripta Metall.* **19**, 539 (1985).
12. A. A. Duswalt, *Thermochim. Acta* **8**, 57 (1974).
13. H. E. Kissinger, *Anal. Chem.* **29**, 1702 (1957).
14. K. G. Keong, W. Sha, and S. Malinov, *J. Alloy. Compd.* **334**, 192 (2002).
15. J.-W. Yoon and S.-B. Jung, *J. Alloy. Compd.* **376**, 105 (2004).
16. C. Schmetterer, H. Flandorfer, Ch. Luef, A. Kodentsov, and H. Ipser, *J. Electron. Mater.* **38**, 10 (2009).
17. J. W. Yoon and S. B. Jung, *J. Alloy. Compd.* **396**, 122 (2005).
18. M. Yamakami and M. Kajihara, *Mater. Trans.* **50**, 130 (2009).
19. J. Wojewoda-Budka, Z. Huber, L. Litynska-Dobrzynska, N. Sobczak, and P. Zieba, *Mater. Chem. Phys.* **139**, 276 (2013).
20. A. Wierzbicka-Miernik, J. Wojewoda-Budka, and P. Zieba, *Sci. Technol. Weld. J.* **17**, 32 (2012).
21. A. Wierzbicka-Miernik, K. Miernik, J. Wojewoda-Budka, K. Szyszkiewicz, R. Filipek, L. Litynska-Dobrzynska, A. Kodentsov, and P. Zieba, *Mater. Chem. Phys.* **142**, 682 (2013).